

## THREE-DIMENSIONAL STUDY OF VORTICAL STRUCTURE AROUND A CUBIC BLUFF BODY IN A CHANNEL

*UDC 532.13 532.551*

**Kurosh Sedighi, Mousa Farhadi**

School of Mechanical Engineering, Mazandaran University, P.O.Box 484  
Babol, Mazandaran, Iran  
mousafarhadi@myway.com

**Abstract.** *A numerical investigation of turbulent flow over wall-mounted cube in a channel was studied by Large Eddy Simulation. The Selective Structure Function model was used to determinate eddy viscosity appears in the subgrid scale stress terms in momentum equation. Studies were carried out for the flows with Reynolds number ranging from 1000 to 40000. To evaluate the computation results, data was compared with measurement data at  $Re=40000$ , showing a reasonable agreement. In this study the effect of Reynolds numbers on flow characteristics such as time-averaged streamlines, instantaneous vorticity and turbulent intensity were investigated. Results of computations show that the flow with higher Reynolds number has a shorter reattachment length and by increasing the Reynolds number, the number of horseshoe vortex in upstream decreases. The negative vorticity near the solid surface is lifted-up by the positive vorticity in the shear layer and penetrates the positive vorticity region and causes the detachment of a part of the shear layer. When the flow pasted around the wall-mounted obstacle, the different pattern of the streamlines appears at each sides of the cube which is changed by increasing the Reynolds number. With increasing the Reynolds number, turbulent intensity and Reynolds stresses increase at the center of the vortexes and sides of the cube respectively.*

**Key words:** *Large Eddy Simulation; Selective Structure Function; Wall-mounted Cube, Reynolds Effects*

### 1. INTRODUCTION

Vortical structure around a wall-mounted bluff body has been a long-lasting research topic for both academic and practical investigation. Since various types of vortices produced by the protruding surface of an obstacle significantly enhances momentum and heat transfer downstream of the obstacle. Understanding their characteristics is essential for many engineering applications where the vortices play an important role. Most of the research on this topic, however, has been carried out in an open flow domain, even

though there exists a number of practical and numerical applications where a wall-mounted obstacle is present in internal flow.

In this study, flow characteristics such as drag coefficient and physical aspects of the vortical structures generated by a wall-mounted obstacle in internal flow are numerically investigated using the Large Eddy Simulation (LES). Especially, the horseshoe vortices and the hairpin vortices associated with a cubic obstacle mounted on one wall of a channel (Fig. 1) are studied. This specific internal flow has particular importance, such as printed circuit boards with chips mounted, heat exchangers with cooling fins, and turbines with rotor and blades, to name a few. Flows of moderate to high Reynolds numbers up to  $Re=40000$  are considered; here  $Re$  is based on the inlet streamwise mean velocity. Horseshoe vortices are produced by three-dimensional boundary-layer separation around cubic wall-mounted on the channel wall. The boundary layer experiences an adverse pressure gradient in the main flow direction due to the blockage effect of the obstacle. When the adverse pressure gradient is significant, the boundary layer separates and a vortex which wraps around the obstacle and trails off is formed. Its overall shape resembles a horseshoe from which the name of the vortex originates. Horseshoe vortices have been attracting many researchers' attention for decades as they are often observed in junction flows of various types of engineering application; for example: junction of fuselage and wing of an airplane, junction of bridge pier and river bed, and junction of turbine blade and rotor, among others. Horseshoe vortices yield large shear stresses near the junction, and unsteady horseshoe vortices may cause serious damages on the structure due to fatigue and erosion.

There is vast literature concerning experiments done for this geometry [Castro and Robins (1977), Castro (1981), Schofield and Logan (1990) and Larousse *et al.* (1991)]. Among them, comprehensive works are those of Martinuzzi and Tropea (1993) and Hussein and Martinuzzi (1996) for Reynolds number of 40000. Their flow patterns show the very complex flow nature in spite of its simple geometry. Technical limitations of experimental methods cause that all the physical phenomena of flow are not obtained clearly. With the recent advent of powerful computers and efficient numerical algorithms, researchers have been carrying out numerical simulations to supplement the drawbacks of experimental techniques. To predict turbulent flow behavior over a wall-mounted cube in a channel, various numerical approaches have been proposed. One of them is the Large Eddy Simulation (LES) which tries to simulate the largest scales of motion while treating the small scales by model. It was appropriate for the flow over a cube to be treated by the LES, as there are large vortices generated in such a flow. Large researchers studied this flow filed with different LES models. Shah and Ferziger (1997) were among the pioneers in doing the LES of flow over a surface mounted cube at Reynolds number 40000, with good correspondence to compare with experiment. This geometry was investigated in the Rottach-Egren workshop (Rodi *et al.* (1995)) and recently by Krajnovic and Davidson (2002a and 2002b), Rahnama and Farhadi (2004) and Farhadi and Rahnama (2006) at Reynolds number 40000 with different LES models. Their results showed that the LES models are capable of this flow field with acceptable accuracy even for coarse grid points (Krajnovic and Davidson (2002a) and Farhadi and Rahnama (2006)). So far a limited numerical study has been carried out on vortical structure of flow over wall-mounted cubic obstacle. Krajnovic and Davidson (2002a and 2002b) and Farhadi and Rahnama (2006) showed the structure of vortexes around the cube with the Second Invariant technique (Jeong and Hussein (1995)) for Reynolds number 40000 and the same study was

done at Reynolds number 1000 by Farhadi and Rahnama (2003). Recently, Hwang and Yang (2004) have studied the vortical structures of flow around a wall-mounted cube in a channel at low to moderate Reynolds numbers up to 3500 using the Direct Numerical simulation (DNS). Their results showed that as the Reynolds number increases, the structure of the horseshoe vortex system becomes complex, and the number of vortices increases in pairs. In the case of a turbulent wake, however, it was observed that the flow becomes less coherent in the near-wall region downstream of the obstacle. Instead, coherent structures such as lateral and hairpin vortices are found present in the vicinity of the two lateral faces of the cube and in the turbulent near-wake region, respectively. The present study investigated the vortical structure of flow from moderate to high Reynolds number by the LES which with the knowledge of authors has not been reported..

## 2. MATHEMATICAL MODEL

In the LES approaches the larger three-dimensional unsteady turbulent motions are directly represented, whereas the effect of small scales of motion is modeled. To do this, a filtering operation is introduced to decompose the velocity vector ( $u_i$ ) into the sum of a filtered (or resolved) component,  $\bar{u}_i$  and a residual (or subgrid-scale) component ( $u'_i$ ). This operation can be represented with a filter of width  $\Delta x$  such that convolution of any quantity  $f(x_i, t)$  by filter function  $G_{\Delta x}(x_i)$  is in the form:

$$\bar{f}(x_i, t) = \int f(y_i, t) G_{\Delta x}(x_i - y_i) dy_i, \quad f' = f - \bar{f} \quad (1)$$

The equations for evolution of the filtered velocity field are derived from the Navier-Stokes equations. These equations are of the standard form, with the momentum equation containing the residual stress tensor. Application of the filtering operation to the continuity and Navier-Stokes equations gives the resolved Navier-Stokes equations, which, in non-dimensional incompressible form, are:

$$\frac{\partial \bar{u}_i}{\partial x_i} = 0 \quad (2)$$

$$\frac{\partial \bar{u}_i}{\partial t} + \frac{\partial}{\partial x_j} (\bar{u}_i \bar{u}_j) = -\frac{\partial \bar{P}}{\partial x_i} + \frac{1}{\text{Re}} \nabla^2 \bar{u}_i - \frac{\partial \tau_{ij}}{\partial x_j} \quad (3)$$

Where  $\bar{P}$  is the pressure,  $\bar{u}_1$ ,  $\bar{u}_2$  and  $\bar{u}_3$  are the streamwise, cross-stream and spanwise components of velocity, respectively. These govern the dynamics of the large, energy-carrying scales of motion. Reynolds number is defined as  $U_{mean}H/\nu$ , where  $U_{mean}$  and  $H$  are the average velocity of entrance profile and cube height, respectively. The effect of small scales upon the resolved part of turbulence appears in the subgrid scale (SGS) stress term,  $\tau_{ij} = \overline{u_i u_j} - \bar{u}_i \bar{u}_j$ , which must be modeled.

The main effect of the subgrid-scale stresses is dissipative around the cut-off spectrum, i.e. to withdraw energy from the part of the spectrum that can be resolved. One model for subgrid-scale stress term  $\tau_{ij}$  is based on its dependence to filtered strain rate through an eddy-viscosity:

$$\tau_{ij} = \nu_t \left( \frac{\partial \bar{u}_i}{\partial x_j} + \frac{\partial \bar{u}_j}{\partial x_i} \right) + \frac{1}{3} \tau_{kk} \delta_{ij} \quad (4)$$

In this study, the eddy viscosity ( $\nu_t$ ) was evaluated using subgrid-scale (SGS) model of Structure Function (SF) and Selective Structure Function (SSF) models. In the Structure Function model, the eddy viscosity is evaluated according to (Métais and Lesieur (1992)):

$$\nu_t^{SF}(\mathbf{x}, \Delta c, t) = 0.105 C_k^{-3/2} \Delta c \sqrt{F_2(\mathbf{x}, \Delta c, t)} \quad (5)$$

Where  $\Delta c = (\Delta x_1 \times \Delta x_2 \times \Delta x_3)^{1/3}$  is the geometric mean of the meshes in the three spatial directions.  $C_k$  is Kolmogorov constant and  $F_2$  is the local structure function constructed with the filtered velocity field  $\bar{\mathbf{u}}(\mathbf{x}, t)$ :

$$F_2(\mathbf{x}, \Delta c, t) = \frac{1}{6} \sum_{i=1}^3 \left( \frac{[\bar{\mathbf{u}}(\mathbf{x}, t) - \bar{\mathbf{u}}(\mathbf{x} + \Delta x_i, t)]^2}{[\bar{\mathbf{u}}(\mathbf{x}, t) - \bar{\mathbf{u}}(\mathbf{x} - \Delta x_i, t)]^2} \right) \left( \frac{\Delta c}{\Delta x_i} \right)^{2/3} \quad (6)$$

$F_2$  was calculated with a local statistical average of square (filtered) velocity differences between  $\mathbf{x}$  and the six closest points surrounding  $\mathbf{x}$  on the computational grid. In some cases, the average may be taken over four points parallel to a given plane. In the Selective version of the Structure Function model, the eddy viscosity was switched off in the regions where the flow is not three-dimensional enough. The three-dimensional criterion was as the following: one measures the angle ( $\alpha$ ) between the vorticity at a given grid point and the average vorticity at the six closest neighboring points (or the four closest points in the four-point formulation). If this angle was less than  $20^\circ$ , the most probable value according to simulations of isotropic turbulence at the resolution of  $32^3$ - $64^3$ , the eddy viscosity is cancelled and only molecular dissipation acts. In this situation the flow is locally close to a two-dimensional state. As compared to the original SF model, this subgrid-scale model dissipates the resolved scale energy at fewer points of the computational domain and the model constant of 0.105 (see equation (5)) has then to be increased to satisfy energy conservation. It was calculated by requiring the eddy viscosity given by the SSF model averaged over the entire computational domain to equal to the corresponding one obtained with the SF model. One finds that the constant in equation (5) has to be multiplied by 1.56 (Lesieur and Métais (1996)).

$$\nu_t^{SSF}(\mathbf{x}, \Delta c, t) = 0.1638 \Phi_{20^\circ}(\mathbf{x}, t) C_k^{-3/2} \Delta c [F_2(\mathbf{x}, \Delta c, t)]^{1/2} \quad (7)$$

Where  $\Phi_{20^\circ}(\mathbf{x}, t)$  is the indicating function based on the value of ( $\alpha$ ):

$$\Phi_{20^\circ}(\mathbf{x}, t) = \begin{cases} 1 & \text{if } \alpha \geq 20^\circ \\ 0 & \text{if } \alpha < 20^\circ \end{cases} \quad (8)$$

Farhadi and Rahnama (2006) showed a smooth varying function rather than an abrupt cut-off. This can predict the distribution of energy between small and large eddies better than standard form of this function, so  $\Phi'_{20^\circ}(\mathbf{x}, t)$  used instead of  $\Phi_{20^\circ}(\mathbf{x}, t)$  which defined as:

$$\Phi'_{20^\circ}(\mathbf{x}, t) = \begin{cases} 0 & \text{for } \alpha < 10^\circ \\ e^{-\left(\frac{d\alpha}{3}\right)^2} & \text{for } 20^\circ \geq \alpha \geq 10^\circ \text{ and } d\alpha = |\alpha - 20^\circ| \\ 1 & \text{for } \alpha > 20^\circ \end{cases} \quad (9)$$

### 3. NUMERICAL METHOD AND COMPUTATIONAL DOMAIN

The governing equations presented in the preceding section were discretized using a finite volume method with staggered grid. The convective terms were discretized using the QUICK scheme. The QUICK scheme has some deficiencies such as numerical dissipation as compared with the Central Difference (CD) scheme; however, it has already been used in the LES simulation of flow over a bluff body (Rodi *et al.* (1995), Farhadi and Rahnama (2003) and Farhadi and Rahnama (2006)). An important issue in the LES computations was that of using at least second order accuracy of both time and spatial discretization of the equations, where both the CD and the QUICK show such behavior. Farhadi and Rahnama (2005) showed that the QUICK scheme can predict the turbulent flow field with reasonable accuracy in compared with the results of the CD scheme.

The convective and diffusive fluxes appear in the momentum equations were treated explicitly in present computations. A third order Runge-Kutta algorithm was used for the time integration in conjunction with the classical correction method at each sub-step. The continuity equation (1) and the pressure gradient term in the momentum equation (2) were treated implicitly, while the convective and diffusive terms are treated explicitly. This method, which is called semi-implicit fractional step method, provides an approach that does not use pressure in the predictor step as in the pressure corrector method (such as the well-known SIMPLE family of algorithms). The linear system of pressure is solved by an efficient conjugate gradient method with preconditioning. The computational domain consists of a plane channel with a cubic obstacle of dimension (H) mounted on one of its wall (Fig. 1). Channel height was selected as 2H and the spanwise width of the channel was selected as 7H such that the cube is located in the middle with equal distance to the spanwise boundaries of 3H. The upstream distance from the front side of the cube to the inlet boundary was selected as 3H and the downstream distance was 6H. The boundary conditions used in the present calculations are as follows. The inlet boundary condition was selected as a fully developed turbulent velocity distribution (one-seventh power law). The outlet boundary condition is of convective type with  $U_c$  equals to mean velocity as follows:

$$\frac{\partial u_1}{\partial t} + U_c \frac{\partial u_1}{\partial x_1} = 0 \quad (10)$$

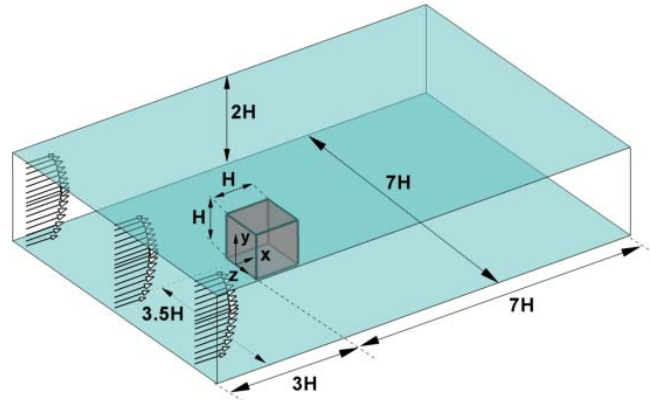


Fig. 1. Geometry of Problem

Obviously, such convective boundary condition is capable of predicting unsteady flow behavior at the exit with good accuracy (Rodi *et al.* (1995)). The spanwise boundary condition was selected as periodic. The minimum grid spacing used in the present computations is 0.03 in all directions adjacent to the cube surface with grid expansion ratio of 1.05 and no-slip boundary condition was used at the wall of cube and channel. The number of grid points used in the present computation, was  $113 \times 51 \times 100$  in the x-, y- and z-direction, respectively. The CFL (Courant-Friedrichs-Lewy) number is less than one for all computations with the maximum value of 0.95. The average time in the simulation was  $200H/U_{\text{mean}}$  where  $H$  is the cube height and  $U_{\text{mean}}$  is the bulk velocity at the inlet. In this study the Reynolds number was selected ranging from 1000 to 40000.

#### 4. RESULTS

Three-dimensional numerical study of turbulent flow over a cubic wall-mounted obstacle in a channel was investigated by the Large Eddy Simulation. To evaluate the results of computational data, the numerical data compared with the measurement data of Martinuzzi and Tropea (1993) and Hussein and Martinuzzi (1996) at Reynolds number 40000 which showed a reasonable agreement. Fig. 2 shows the time-averaged streamwise, cross stream velocity and turbulent kinetic energy profiles in different positions at the plane  $z=0$  compared with the experiment. It is observed that the results of computational data show reasonable accuracy especially for streamwise and cross stream velocity profiles. It should be mentioned that although some discrepancies exist at the turbulent kinetic energy profiles, the numerical data follow the trend of experiment. Probability is due to the use of the coarse grid resolution near the wall. In this area, energy transfers from large to small scale eddies that can be capable by using fine grid resolution in this region. Furthermore, the difference between numerical and experimental data in the length and form of the recirculation zones may be creating these discrepancies.

Figure 3 shows time-averaged streamlines at the floor of the channel for various cases of Reynolds numbers. The blockage effect of the obstacle creates an adverse pressure gradient which makes the flow separate and trail off along the obstacle, forming a horseshoe vortex. For all Reynolds numbers, horseshoe vorticity does appear at the upstream and trail around the obstacle. At the low Reynolds number, the time-averaged streamlines show a very complex structure with the several horseshoe vortices (Fig. 4). In addition, at the lateral sides of the cube, there are two saddle points (arrows in the Fig. 3) for all Reynolds numbers, which are also observed in the oil visualization of Martinuzzi and Tropea (1993). With increasing the Reynolds number, the structure and number of horseshoe vortex were changed. By increasing the Reynolds number, the middle horseshoe vortex disappeared and the other two horseshoe vortex merged together.

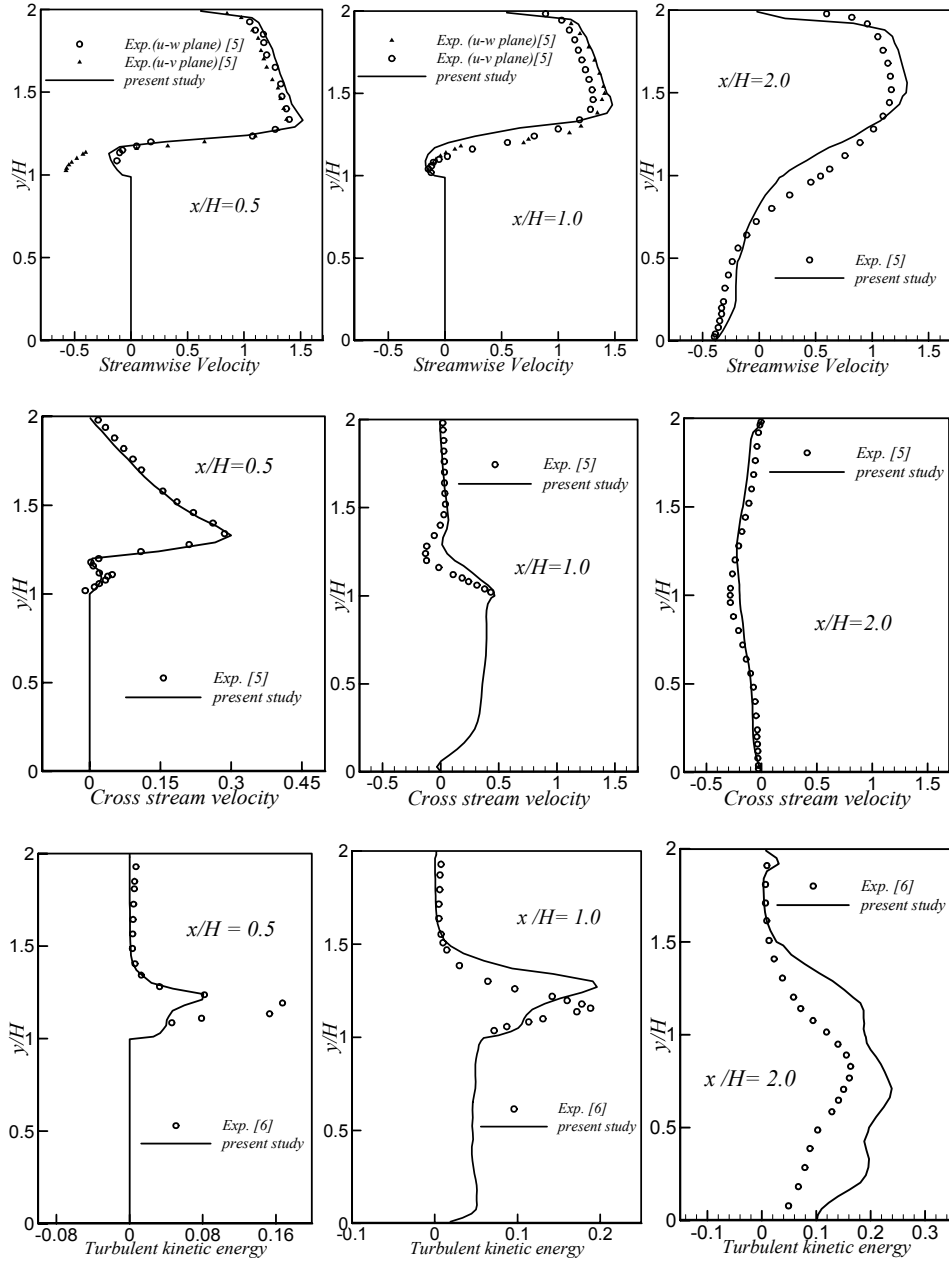


Fig. 2. Time-averaged Streamwise, Cross-stream Velocity and Turbulent Kinetic Energy Profiles Compared with Experiment at the Plane  $z=0$  at Reynolds Number 40000

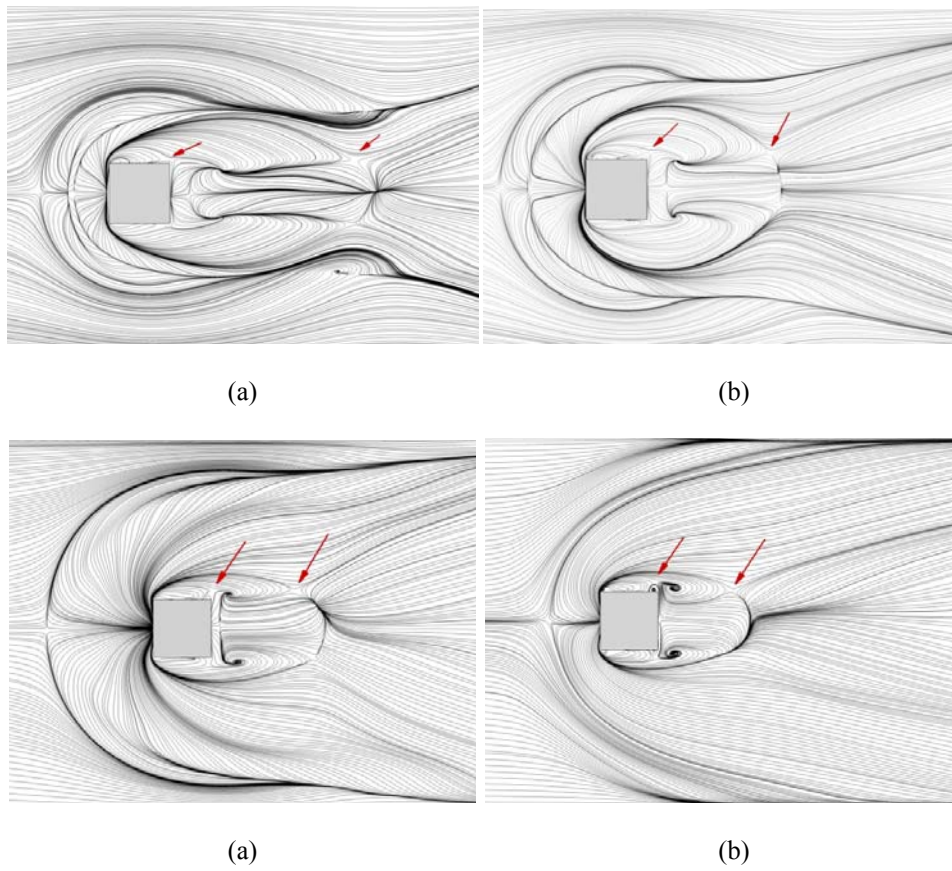


Fig. 3. Time-averaged Streamlines at the Floor of the Channel for Reynolds Number (a) 1000, (b) 3200, (c) 10000 and (d) 40000

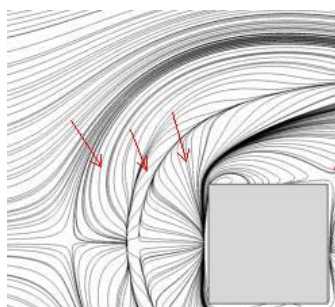


Fig. 4. Time-averaged Streamlines at the Floor of the Channel for Reynolds Number 1000



One of the complex phenomena in the flow over a cube in a channel is the formation of vortices and their subsequent stretching. The sequence presented in the Fig. 5 shows the development and interactions of vorticity regions with the solid surfaces on the roof of the obstacle. It is clear that shear layer forms on the roof of the obstacle. This layer consists of the vortex sheet with positive vorticity that is separated from the roof. As we follow these sequences, it can be seen that the positive vorticity starts to accumulate and strengthens over certain part. The interaction of the accumulate vorticity with a solid surface causes the formation of the negative vorticity at the roof. The negative vorticity is lifted-up by the positive vorticity in the shear layer. This negative vorticity penetrates the positive vorticity region and causes the detachment of a part of the shear layer.

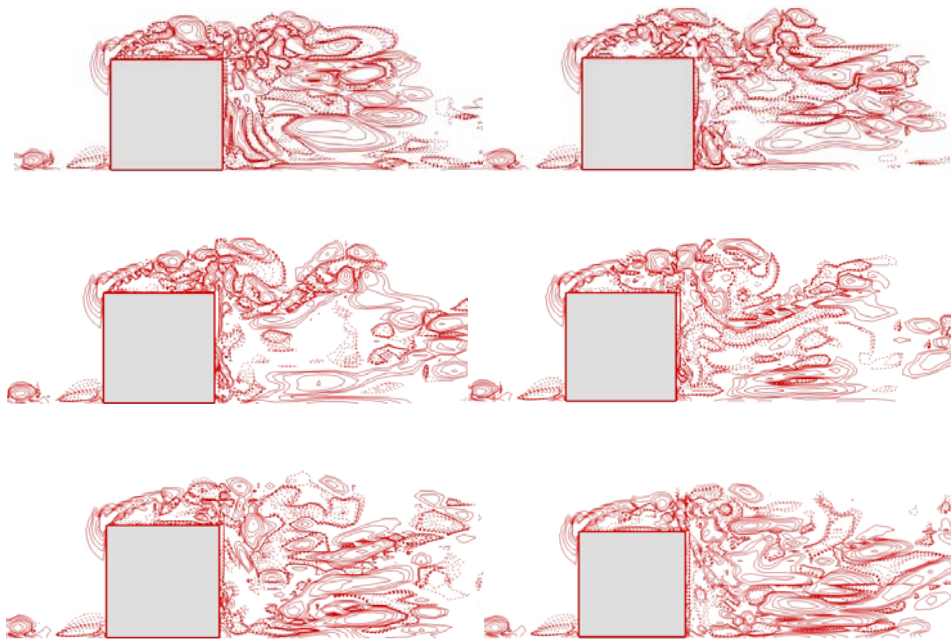


Fig. 5. Instantaneous Contours of Positive (Solid Lines) and Negative (Dashed Lines) Value of  $W_z$  at the Center Line of the Channel for Reynolds Number 3200. The Increment is  $tU_{\text{mean}}/H=0.5$

As can be seen in the Fig. 6 the same mechanism described above is repeated at the side of the obstacle. It is clear that accumulation and strengthening of positive vorticity leads to the generation of negative vorticity on the wall of the obstacle. The interaction of the positive and negative vorticity regions causes the penetrating of the positive vorticity.

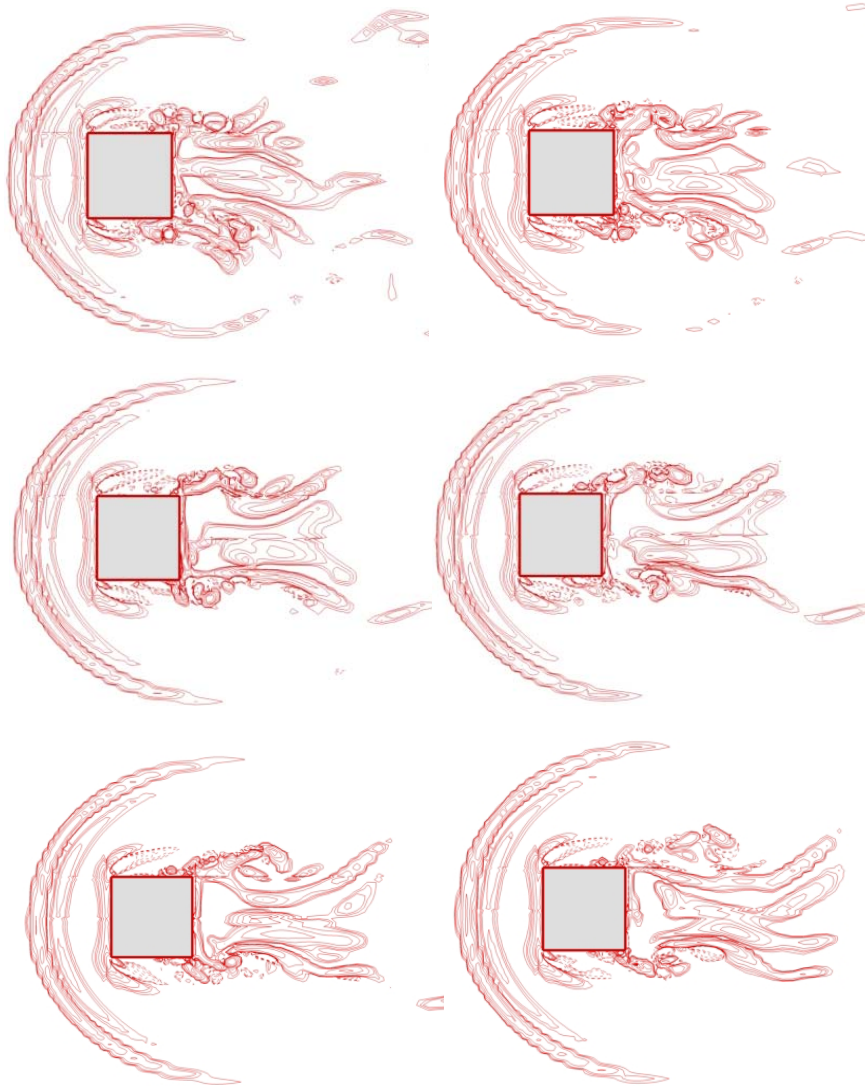


Fig. 6. Instantaneous Contours of Positive (Solid Lines) and Negative (Dashed Lines) Value of  $Wz$  at the Floor of the Channel for Reynolds Number 3200. The Increment is  $tU_{\text{mean}}/H=0.5$

In the Fig. 5, the hairpin vortex at the front side of the cube is nearly steady because the steady behavior of flow field. As the flow passes the rear edge of the obstacle, the shear layer becomes unstable and a new vortex head is born while the existing vortex head is convected downstream and dissipated. The structure and shape of horse shoe vortex are nearly steady at the floor of the channel (Fig. 6). When the flow passed around the wall-mounted obstacle, the different pattern of the streamlines appears at the each sides of the cube which changed by increasing the Reynolds number. Fig. 7 shows the time-

averaged streamlines on each face of the obstacle at different Reynolds numbers. From this figure, one can deduce the separation and reattachment structure at each face of the cube. At the front side of the cube, one reattachment point was observed which was similar for all Reynolds numbers.

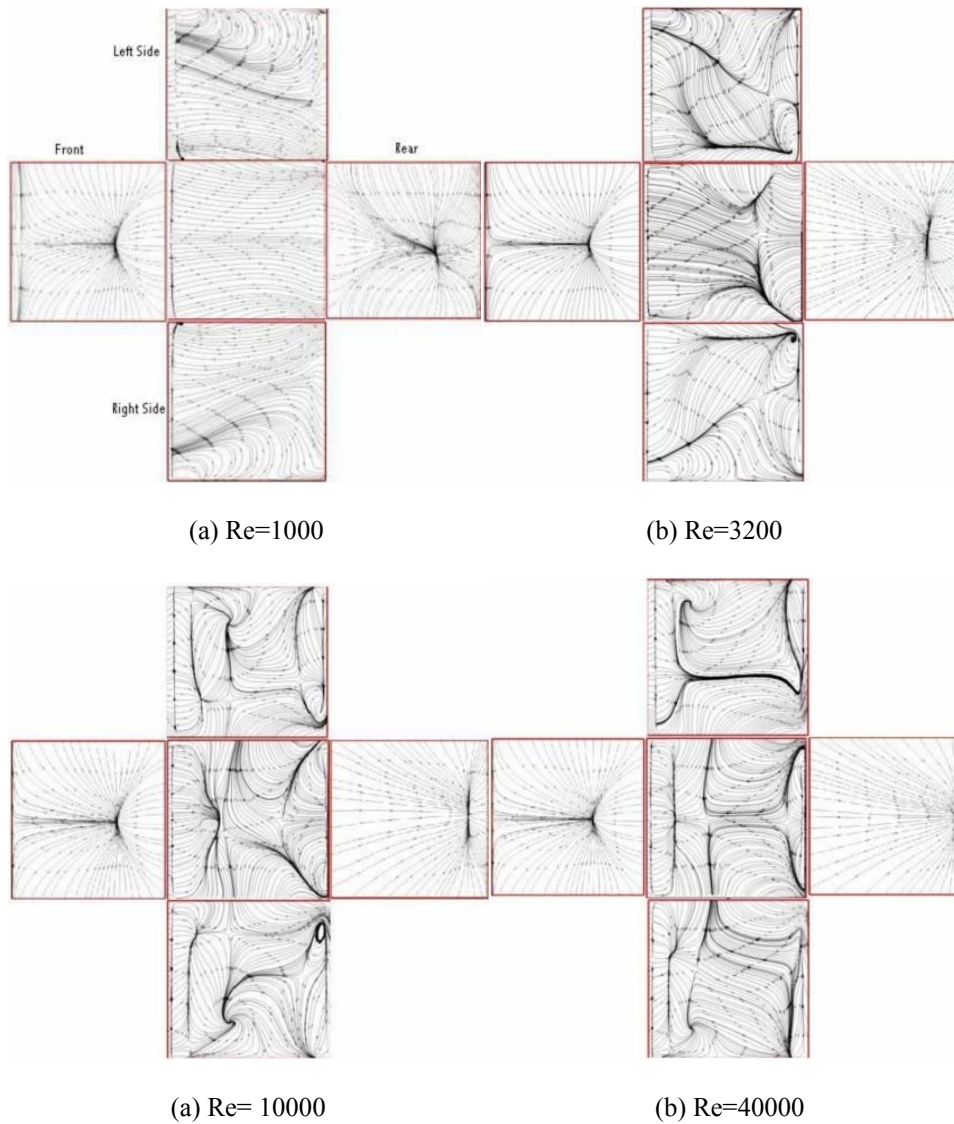


Fig. 7. Time-averaged Streamlines on Each Face of the Obstacle for Different Re Numbers

It should be mentioned that the small separation line appears near the floor of the channel at the Reynolds number 1000 and then disappears with increasing the Reynolds number. At the rear of the obstacle, there is only one reattachment point on the surface of the

cube which moves toward the floor of the channel with increasing the Reynolds number. At the top and sides of the cube the flow pattern becomes more complex except for Reynolds number 1000. It is observed that the separation line exists at all Reynolds numbers and several reattachment points do appear, that increase by increasing the Reynolds number. Fig. 8 shows variation of time-averaged contours of turbulent kinetic energy for different Reynolds numbers at the centerline of the cube (plane  $z = 0$ ). It is observed that the maximum turbulent intensity was at the center of the recirculation zone in the downstream of the cube. This caused maximum velocity at the center of the vortex core. With the increasing Reynolds number, the recirculation center moves towards the rear of the cube so the maximum intensity of the turbulence shifts to the wall of the cube. It should be mentioned that the maximum quantity of the turbulent kinetic energy increases with increasing the Reynolds number.

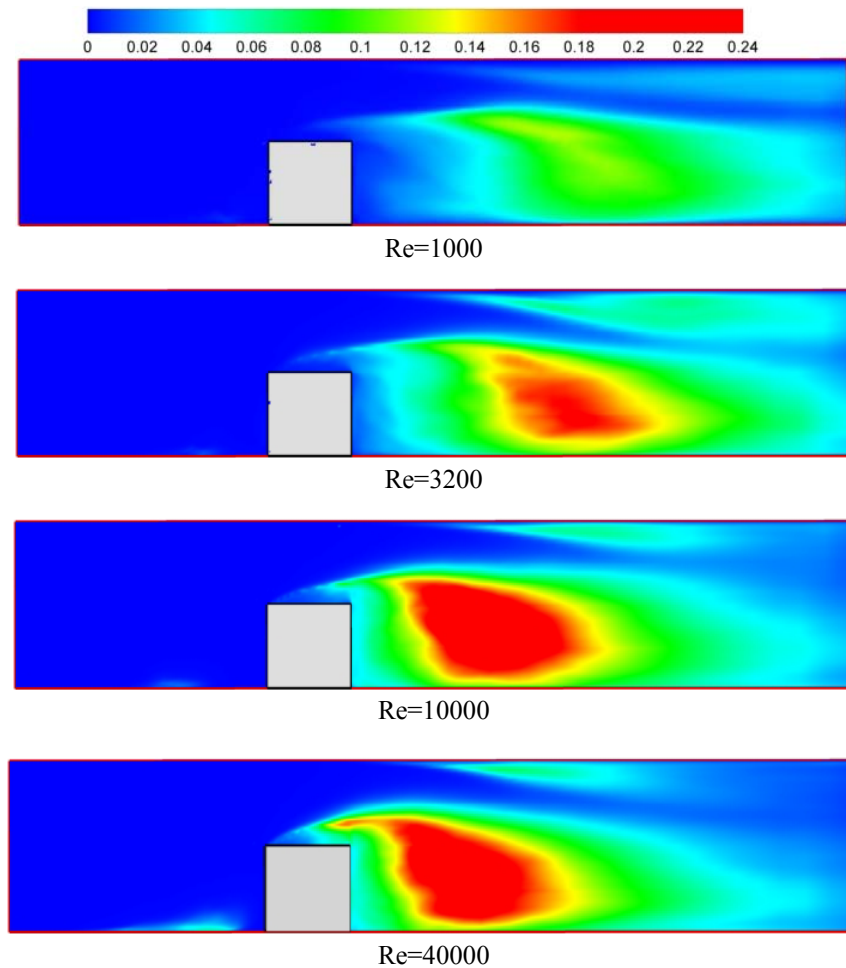


Fig. 8. Time-averaged Contours of Turbulent Kinetic Energy at the Centerline of the Cube for Different Reynolds Numbers

Stresses fluctuated between negative and positive values depending on the vortex structure around the wall-mounted obstacle. Fig. 9 shows time-averaged contours of magnitude of Reynolds stress ( $u'v'$ ) at the centerline of the channel for different Reynolds numbers. Hence, there was a small positive value immediately behind the obstacle due to the small corner vortex. Values became strongly negative within the recirculation region and more strongly positive as the flow reattached and recovered. This phenomena was observed in other studies of flow over wall-mounted obstacle (Keylocka *et al.*(2005)).The LES was able to detect the presence of favorable and adverse pressure gradients at the wall as the flow expanded and contracted over the obstacle. A steady-state numerical method would not resolve these aspects of the flow, leading to inaccuracies in the estimation of recirculation zone statistics and the effect of the bed-mounted obstacle on downstream flow mixing and instantaneous bed forces (Keylocka *et al.* (2005))

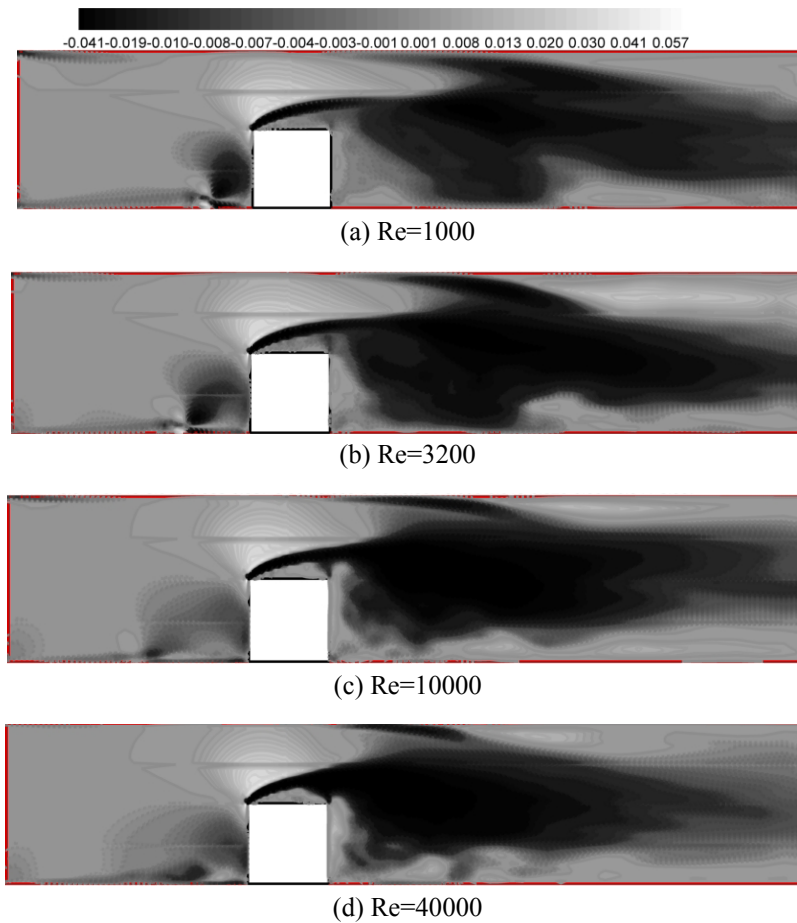


Fig. 9. Time-averaged Contours of Magnitude of Reynolds Stress ( $u'v'$ ) at the Center Line of the Channel at Different Reynolds Numbers

Fig. 10 shows the time-averaged Reynolds stress contours at the floor of the channel for different Reynolds numbers. It is observed that the blockage effect of the obstacle creates an adverse pressure gradient which makes the flow separate and trail off along the obstacle, forming a horseshoe vortex. One can identify a horseshoe-shaped region of strong shear stress around the obstacle, whose magnitude is approximately several times larger than its surrounding. As the Reynolds number increases, the number of horseshoe vortex decreases, so it can be observed that the maximum value of  $u'v'$  only occurs at the sides of the cube.

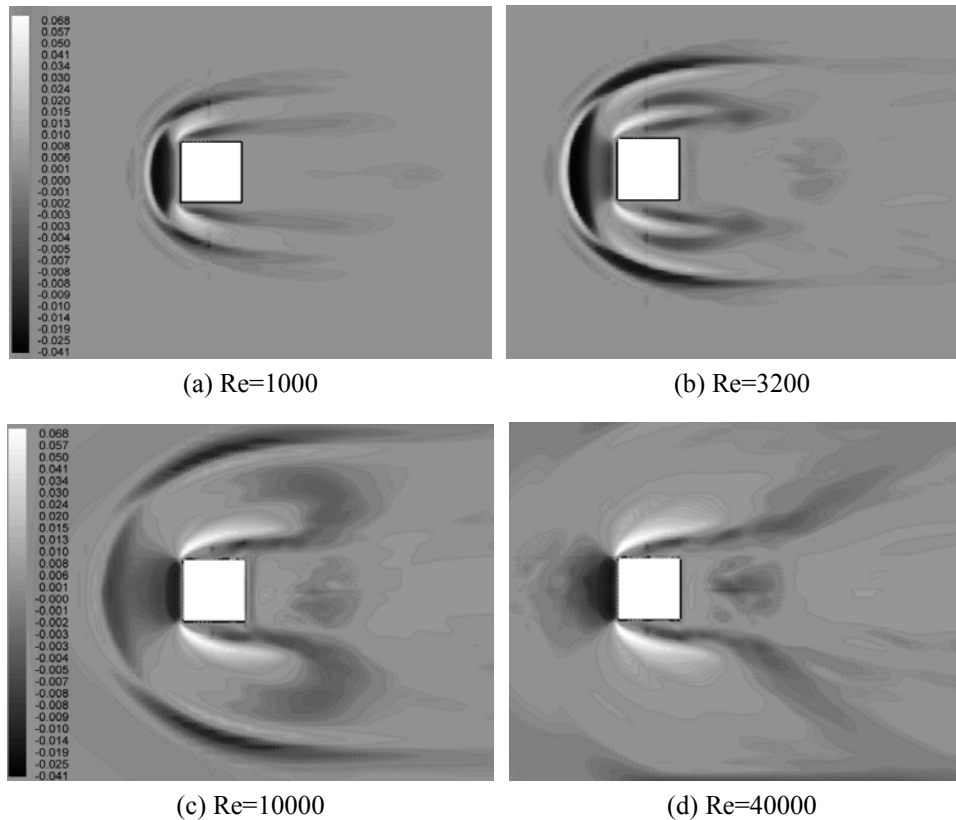


Fig. 10. Time-averaged Contours of Magnitude of Reynolds Stress ( $u'v'$ ) at the Floor of the Channel at Different Reynolds Numbers

## 5. CONCLUSION

The effects of the Reynolds number on turbulent flow over wall-mounted cube in a channel were numerically investigated using the Large Eddy Simulation. Studies were carried out for the flows with the Reynolds number ranging from 1000 to 40000. The blockage effect of the obstacle creates an adverse pressure gradient caused the flow separation and trailed off along the obstacle forming a horseshoe vortex. For all the

Reynolds numbers, horseshoe vorticity does appear at the upstream and trails around the obstacle. Results of computations show that the flow with a higher Reynolds number has a shorter reattachment length. By increasing the Reynolds number, the number of horseshoe vortex in upstream decreases. The interaction of the accumulated vorticity with the solid surface caused the formation of the negative vorticity which is lifted-up by the positive vorticity in the shear layer. This negative vorticity penetrates the positive vorticity region and causes the detachment of a part of the shear layer. The hairpin vortex at the front side of the cube is nearly steady that because of the steady behavior of flow field. When the flow pasted around the wall-mounted obstacle, the different pattern of the streamlines appears at the each sides of the cube which is changed by increasing the Reynolds number. With increasing the Reynolds number, turbulent intensity and Reynolds stresses increase at the center of the vortexes and sides of the cube respectively.

## REFERENCES

1. Castro, I. P. and Robins, A. G., 1977, *The flow around surface-mounted cube in uniform and turbulent streams*, J. of Fluid Mech., 79(2), pp.307-335.
2. Castro, I. P., J., 1981, *Measurements in shear layers separating from surface-mounted bluff bodies*, J. of Wind Eng. and Ind. Aerodynamics, 7, pp. 253-272.
3. Farhadi, M., Rahnama, M., 2005, *Three-dimensional study of separated flow over a square cylinder by large eddy simulation*, Journal of Aerospace Engineering (Proceeding of the Institution of Mechanical Engineers Part G), 219(3), pp. 225-234.
4. Farhadi, M., Rahnama, M., 2003, *Large eddy simulation of flow over a wall-mounted cube at moderate Reynolds number*, Journal of Engineering, 2(3&4), pp. 193-202.
5. Farhadi, M., Rahnama, M., 2006, *Large Eddy Simulation of Separated Flow over a Wall-Mounted Cube*, Int. J. of Science and Technology, 13(2), pp. 124-133.
6. Ferziger, J. H., Peric, M., 1996, *Computational methods for fluid dynamics*, Springer, Germany, 2<sup>nd</sup> ed., 273 pp.
7. Hussein, H. J. and Martinuzzi, R. J., 1996, *Energy balance for turbulent flow around a surface mounted cube placed in a channel*, Phys. Of Fluids, 8, pp. 764-780.
8. Hwang, J. Y., Yang, K. S., 2004, *Numerical study of vortical structures around a wall-mounted cubic obstacle in channel flow*, Physics of Fluids, 16 (7), pp. 2382-2394.
9. J. Jeong, F. Hussein, 1995, *On the identification of a vortex*, J. of Fluid. Mech., 285, pp. 69-94.
10. Keylocka, C. J., Hardyb, T. R. J., Parsons, D. R., Fergusonb, R. I., Laneb, S. N., and Richardsd, K. S., 2005, *The theoretical foundations and potential for Large-Eddy Simulation (LES) in fluvial geomorphic and sedimentological research*, Earth-Science Reviews, 71, pp. 271–304.
11. Krajnovic, S., Davidson, L., 2002, *A mixed one-equation subgrid model for large-eddy simulation*, Int. J. Heat Fluid Flow, 23, pp. 413-425.
12. Krajnovic, S., Davidson, L., 2002, *Large eddy simulation of the flow around a bluff body*, AIAA Journal, 40(5), pp. 927-936.
13. Larousse, A., Martinuzzi, R., and Tropea, C., 1991, *Flow around surface-mounted, three-dimensional obstacles*, 9th Int. Sym. on Turbulent Shear Flow, Springer-Verlag, pp. 127–139.
14. Lesieur, M., Métais, O., 1996, *New trends in LES of turbulence*, Ann. Rev. of Fluid Mechanics, 28, pp. 45-82.
15. Martinuzzi, R. and Tropea, C., 1993, *The flow around surface-mounted prismatic obstacles placed in a fully developed channel flow*, ASME J. of Fluids Eng., 115, pp. 85-92.
16. Métais, O., Lesieur, M., 1992, *Spectral large eddy simulations of isotropic and stably-stratified turbulence*, J. of Fluid Mechanics, 239, pp. 157-194.
17. Rahnama, M., Farhadi, M., 2004, *Large eddy simulation of flow over a wall-mounted cube*, Proc. of 12<sup>th</sup> Annual Conf. of Computational Fluid Dynamics, Ottawa, Canada, pp. 708-714.
18. Rodi, W., Ferziger, J. H., Breuer, M. and Pourquie M., 1995, *Workshop on LES of flows past bluff bodies*, Rotach-Egern, Germany, June.

19. Schofield, W. and Logan, E., 1990, *Turbulent shear flow over surface-mounted obstacles*, ASME J. of Fluids Eng., 112, pp. 376-385.
20. Shah, K. B. and Ferziger, J. H., 1997, *A fluid mechanics view of wind engineering: Large eddy simulation of flow past a cubic obstacle*, J. of Wind Eng. and Ind. Aerodynamics, 67 & 68, pp. 211-224.

## **TRODIMENZIONALNO ISTRAŽIVANJE VRTLOŽNE STRUKTURE OKO ISKOŠENE KOCKE U JEDNOM KANALU**

**Kurosh Sedighi, Mousa Farhadi**

*Numeričko istraživanje turbulentnog toka preko kocke montirane na zid u jednom kanalu izučavala je Simulacija velikog vrtloga. Model selektivne funkcije strukture se koristi za ispitivanje viskoznosti vrtloga i on se javlja u članovima jednačine momenta u podrešetkastom naprezanju. Istraživanja su vršena za protoke sa Reynoldsovim brojem od 1000 do 40000. Za procenu kompjuterskih podataka podaci su upoređivani sa podacima merenja pri  $Re=40000$  i pokazali su dobro slaganje. U ovom istraživanju ispitivan je uticaj Reynoldsovih brojeva na karakteristike toka kao što su vremenski uprosečene linije toka, trenutna vrtlogivost i intenzitet turbulencije. Rezultati izračunavanja pokazuju da Reynoldsov broj ima kraću dužinu ponovnog pričvršćivanja dok povećanjem Reynoldsovog broja opada broj vrtloga u obliku potkovice u gornjem toku. Negativna vrtlogivost pored čvrstog tela raste sa pozitivnom vrtlogljivošću u sloju smicanja i prodire u region pozitivne vrtlogljivosti izazivajući odvajanje jednog dela sloja smicanja. Kada se tok veže oko prepreke na zidu, javlja se drugačiji obrazac linija toka na svakoj strani kocke što se, pak, menja promenom Reynoldsovog broja. Sa povećanjem Reynoldsovog broja, intenzitet turbulencije i Reynoldsov napon se povećavaju u centru vorteksa i na stranama kocke, respektivno.*

*Ključne reči: Simulacija velikih vrtloga, selektivna funkcija strukture, kocka montirana na zidu, Reynoldsov efekat*